Climate Dynamics (2004) 23: 859–868
DOI 10.1007/s00382-004-0470-5

Aiming Wu · William W. Hsieh

The nonlinear association between ENSO and the Euro-Atlantic winter sea level pressure

Received: 3 February 2004 / Accepted: 19 July 2004 / Published online: 11 August 2004

Abstract A nonlinear projection of the tropical Pacific sea surface temperature anomalies (SSTA) onto the Northern Hemisphere winter sea level pressure (SLP) anomalies by neural networks (NN) was performed to investigate the nonlinear association between El Niño-Southern Oscillation (ENSO) and the Euro-Atlantic winter climate. While the linear impact of ENSO on the Euro-Atlantic winter SLP is weak, the NN projection reveals statistically significant SLP anomalies over the Euro-Atlantic sector during both extreme cold and warm ENSO episodes, suggesting that the Euro-Atlantic climate mainly responds to ENSO nonlinearly. The nonlinear response, mainly a quadratic response to the SSTA, reveals that regardless of the sign of the SSTA, positive SLP anomalies are found over the North Atlantic, stretching from eastern Canada to Europe (with anomaly center located just northwestward of Portugal), and negative anomalies centered over Scandinavia and Norwegian Sea, consistent with the excitation of the positive North Atlantic Oscillation pattern.

1 Introduction

Numerous studies have been devoted to documenting and understanding the impact of the El Niño-Southern Oscillation (ENSO) phenomenon on global climate variability since the early 1980s (Trenberth et al. 1998). An important progress on this issue made in recent years is that the extratropical climate response to the tropical Pacific sea surface temperature (SST) anomalous forcing is found to be nonlinear. Observational study and numerical models have demonstrated that North America wintertime climate has asymmetric response patterns during opposite phases of ENSO (e.g. Shabbar et al. 1997; Montroy et al. 1998; Hoerling et al. 1997, 2001a; Wu et al. 2003). A major characteristic of North America climate response to ENSO is that there is an eastward phase shift of the circulation anomalies (by about 35°) between the composites of warm ENSO episodes and the composites of cold episodes, with two wave trains originating from different tropical sources (Hoerling et al. 1997).

On the other hand, few studies have addressed the question if the impact of ENSO on the Euro-Atlantic climate is nonlinear or not, partially because of the weaker and less robust relationship between ENSO and the North Atlantic Oscillation (NAO, Hurrell et al. 2003). The impact of ENSO on the atmospheric circulation in the North Atlantic region and the temperature in Europe has been examined by some authors (e.g. Rogers 1984; Fraedrich and Müller 1992; Fraedrich 1994; Halpert and Ropelewski 1992; Huang et al. 1998; Dong et al. 2000; Sutton and Hodson 2003), but these studies show varied, even contradictory results. For example, Rogers (1984) concluded from an analysis of historical sea level pressure (SLP) data that there is no significant correlation between indices of the NAO and ENSO on interannual and longer timescales. With a multiresolution cross-spectral technique, Huang et al. (1998), however, found significant coherence between the NAO and Niño3 indices in about 70% of the warm ENSO episodes from 1900 to 1995. Though there is some discrepancy in the location of the atmospheric circulation anomalies, the studies by Pozo-Vázquez et al. (2001) and Cassou and Terray (2001) both found no statistically significant SLP anomaly patterns in the North Atlantic area associated with warm ENSO episodes, but both found a statistically significant SLP anomaly pattern resembling the positive phase of the NAO during cold episodes. A cyclone tracking analysis

A. Wu (✉) · W. W. Hsieh
Department of Earth and Ocean Sciences,
University of British Columbia, Vancouver,
BC, Canada, V6T 1Z4
E-mail: awu@eos.ubc.ca
Tel.: +1-604-8223932
Fax: +1-604-8226088

from a high resolution atmospheric general circulation model (AGCM) simulation reveals a southward shift of the North Atlantic low pressure systems in the winter season during El Niño episodes (Merkel and Latif 2002). The effects of different ocean conditions (including ENSO) on the Northern Hemisphere midlatitude cyclone variability were also discussed by Raible and Blender (2004).

In recent years, neural network (NN) methods have been increasingly applied to study the atmosphere and oceans, with reviews given by Hsieh and Tang (1998) and Hsieh (2004). In this work, the association between ENSO and the Euro-Atlantic climate is investigated by applying a nonlinear projection of the ENSO SST index onto the Northern Hemisphere winter SLP. If x denotes the ENSO SST index, and y, the extratropical atmospheric response to ENSO, the nonlinear response function $y = f(x)$ can be obtained via NNs (Wu and Hsieh 2004) (the nonlinear projection by NN is simply called an *NN projection* thereafter). In traditional linear projection, a linear regression of the atmospheric response variable on the ENSO SST index, yields strictly anti-symmetric atmospheric patterns during El Niño and La Niña (e.g. Deser and Blackmon 1995). In "one-sided regression", one calculates a linear regression between the SST index and the response variable when the SST index is positive, and another linear regression when the SST index is negative (Hoerling et al. 2001a). In contrast, the NN projection detects the fully nonlinear atmospheric response to ENSO. Compared to the nonlinear canonical correlation analysis (NLCCA), developed also via NN (Hsieh 2001), the NN projection has a much simpler NN structure with less model parameters, hence easier to obtain robust results from noisy data. Composite analysis computes the atmospheric patterns by averaging the data over the years when warm episodes occurred, and averaging over cold episodes. While the patterns during warm and cold episodes are not forced to be anti-symmetrical, composite analysis does not give a nonlinear response function.

The data and the method are briefly introduced in Sect.2. The nonlinear SLP anomaly patterns associated with the ENSO SST index detected by the NN projection, and separately by a polynomial fit are presented in Sect. 3. Section 4 gives a summary and discussion.

2 Data and methodology

The monthly SLP data from January 1950 to March 2003 with a 5° by 5° resolution came from the Trenberth Northern Hemisphere SLP data set (Trenberth and Paolino 1980). Anomalies were calculated by subtracting the monthly climatology based on the period 1950–2002. Data from 20°N to the North Pole and during the winter season (December–March) were used, thus the total number of months was 215. After removing the linear trend and weighing the anomalies by the square root of the cosine of the latitude, a principal component analysis (PCA) was used to compress the data, with the 11 leading principal components (PCs, accounting for about 83% of the total variance) retained. Analysis using different number of PCA modes showed that our results were not sensitive to the number of modes as long as 11 or more modes were used.

The spatial patterns of the four leading PCA modes (also called the empirical orthogonal functions, EOFs) are shown in Fig. 1, where EOF1 (Fig. 1a) shows the typical Northern annular mode (NAM) or the Arctic Oscillation (AO, Thompson and Wallace 1998, 2000), and EOF2 reveals strong variability over North Pacific and a dipole structure between the North Atlantic and the Norwegian Sea (Fig. 1b). The EOF3 shows SLP anomalies over the North Atlantic and Russia in opposition to the anomalies over Greenland and Canada (Fig. 1c), while EOF4 displays anomalies over northern Europe in opposition to the anomalies over the remaining mid-high latitude Northern Hemisphere (Fig. 1d).

The monthly SST for the period January 1950 to March 2003 with a resolution of 2°× 2° came from the extended reconstructed sea surface temperatures (ERSST) data set (Smith and Reynolds 2003). The SST anomalies were calculated by subtracting the monthly SST climatology based on the period 1950–2002, and the linear trend removal was performed prior to PCA. The ENSO SST index is defined as the standardized first PC of the winter (December–March) sea surface temperature anomalies (SSTA) over the tropical Pacific (122°E–72°W, 22°S–22°N). This ENSO SST index correlates strongly (> 0.96) with the traditional ENSO SST index of Niño3 and Niño3.4.

While the SST changes in the tropical Pacific have been found to be responsible for the rising trend in the NAO index that was observed after 1950 (Hoerling et al. 2001b), we will focus on the interannual to decadal time scales in this study as the linear trend has been removed from both the SLP and SST data.

A schematic diagram of the feed-forward NN model is shown in Fig. 2. The NN has a single input, the SST index (x), which is nonlinearly mapped to m intermediate variables called hidden neurons, $\mathbf{h} = \tanh(\mathbf{W}^{(x)}x + \mathbf{b}^{(x)})$, where $\mathbf{W}^{(x)}$ and $\mathbf{b}^{(x)}$ are the weight and bias vector respectively ($\mathbf{h}$, $\mathbf{W}^{(x)}$ and $\mathbf{b}^{(x)}$ are column vectors of length m). The NN model then maps from the layer of hidden neurons to 11 output variables $\mathbf{y}' = \mathbf{W}^{(h)}\mathbf{h} + \mathbf{b}^{(h)}$, where $\mathbf{W}^{(h)}$ is a $11\times m$ weight matrix, and $\mathbf{b}^{(h)}$, a bias vector of length 11. With enough hidden neurons, the NN is capable of modelling any nonlinear continuous function to arbitrary accuracy (Bishop 1995). Starting from random initial values, the NN model parameters (in $\mathbf{W}^{(x)}$, $\mathbf{b}^{(x)}$, $\mathbf{W}^{(h)}$ and $\mathbf{b}^{(h)}$) are optimized so that the mean square error (MSE) between the 11 model outputs ($\mathbf{y}'$) and the 11 leading PCs (standardized) of the SLP anomalies ($\mathbf{y}$) is minimized. To avoid local minima during optimization, the NN model was trained repeatedly 30 times

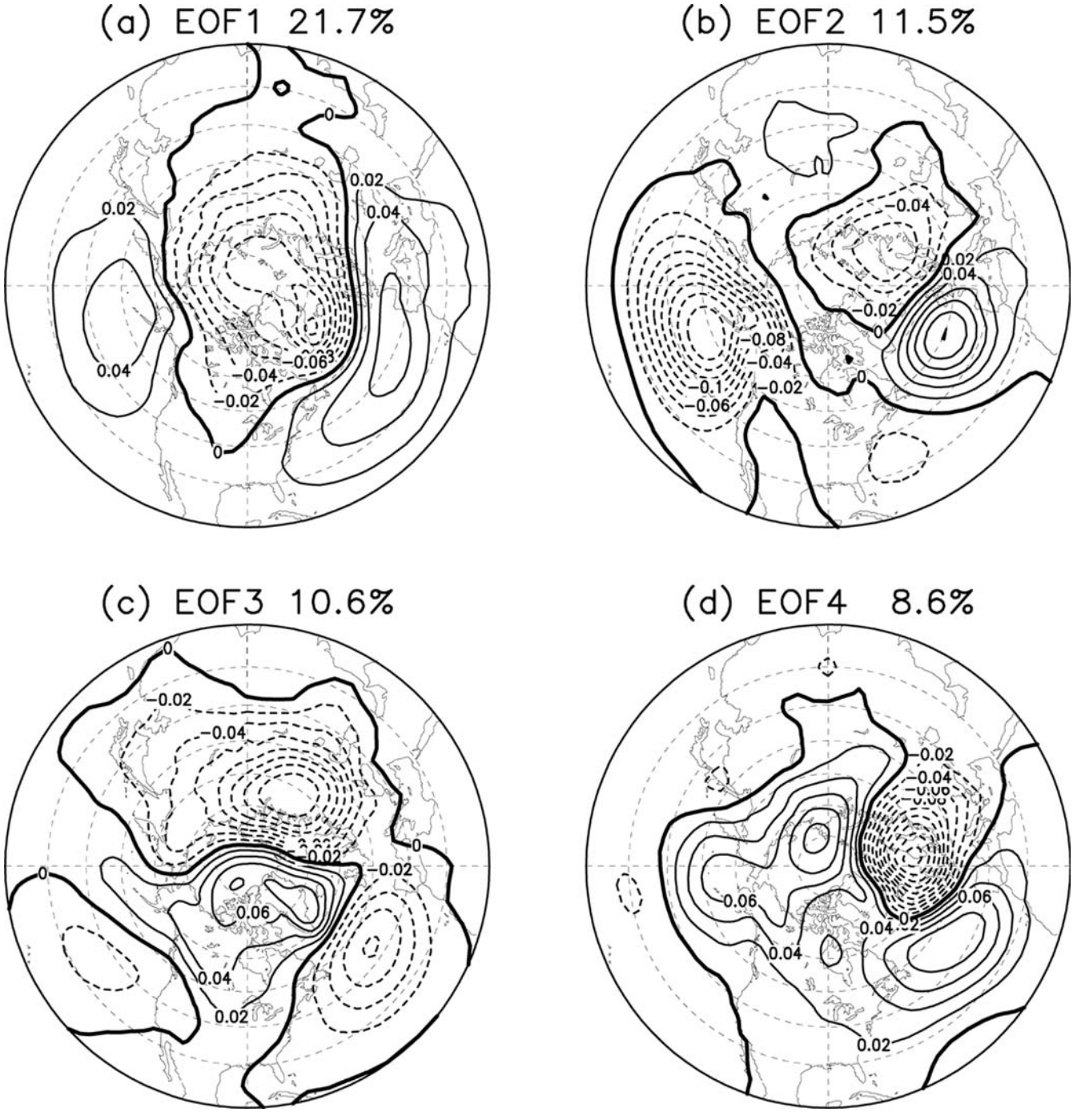

Fig. 1 The four leading EOFs of Northern Hemisphere winter (December–March) SLP anomalies. *Solid curves* denote positive contours, *dashed curves*, negative contours, and *thick curves*, the zero contours. The contour interval is 0.02. The EOFs have been normalized to unit norm, and the percentage variance explained by each EOF is given in the figure title

from random initial parameters and the solution with the smallest MSE was chosen and the other 29 rejected.

To reduce the sampling dependence of a single NN solution, we repeated the above calculation 400 times with a bootstrap approach. A bootstrap sample was obtained by randomly selecting (with replacement) one winter's data record 54 times from the original record of 54 winters, so that on average about 63% of the original record was chosen in a bootstrap sample (Efron and Tibshirani 1993). The ensemble mean of the resulting 400 NN models was used as the final NN solution, found to be insensitive to the number of hidden neurons, which was varied from 1 to 5 in a sensitivity test. Results from using three hidden neurons are presented.

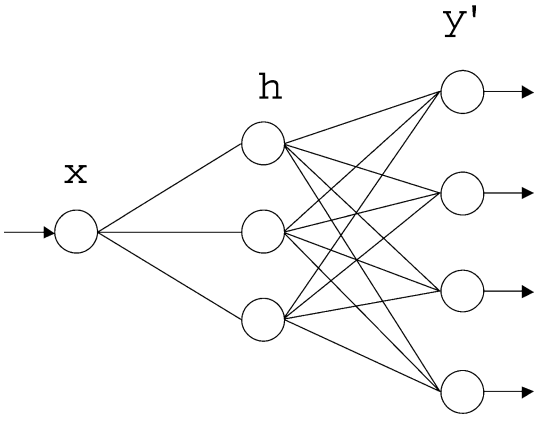

Fig. 2 A schematic diagram of the feed-forward NN model used to perform the nonlinear projection. The NN has a single input x, which is nonlinearly mapped to intermediate variables **h** (called hidden neurons), which are then linearly mapped to the output variables $\mathbf{y}'$. The model parameters are optimized by minimizing the MSE given by the cost function $J = \left\langle \|\mathbf{y} - \mathbf{y}'\|^2 \right\rangle$, where **y** is the observed data. In this study, x is the ENSO SST index, and **y**, the 11 leading PCs (standardized) of the Northern Hemisphere winter SLP anomalies, with three hidden neurons used

3 Results

3.1 SLP response patterns extracted by NN projection

The climate signal extracted by the nonlinear projection is manifested by a curve in the 11 dimensional phase space of the SLP PCs; in contrast, the linear projection extracts a straight line in the same 11-D space. This curve was parabola-like (Fig. 3) when viewed in the PC_1–PC_2 plane and in the PC_1–PC_3 plane, indicating that the SLP response to the SST index is a nonlinear combination of some of its leading PCA modes. For a given value of the SST index, the 11 SLP PC values derived from the NN model can be combined with the corresponding EOFs (Fig. 1) to yield the SLP spatial anomalies associated with this value of the SST index. As the SST index varies, both the pattern and amplitude of the SLP spatial anomalies change, in contrast to the linear projection, which gives a fixed spatial pattern and a variable amplitude.

When the SST index takes on its minimum value (i.e. strong La Niña), besides the positive SLP anomalies over North Pacific (Fig. 4a), we see statistically significant positive SLP anomalies over North Atlantic in a zonal belt stretching from the east coast of North

Fig. 4 The SLP anomalies associated with **a** the minimum SST index and **b** maximum SST index, and with **c** one half of the minimum SST and **d** one half of the maximum SST. The SLP anomalies in panel **a** minus twice the anomalies in **c** are shown in panel **e**, and the anomalies in panel **b** minus twice the anomalies in **d** are shown in panel **f**. If the SLP response to the SST index is strictly linear, then **e** and **f** will show zero everywhere. Contour interval is 1 hPa and the *grey areas* indicate statistical significance at the 5% level, based on the distribution of the results from the 400 bootstrap samples

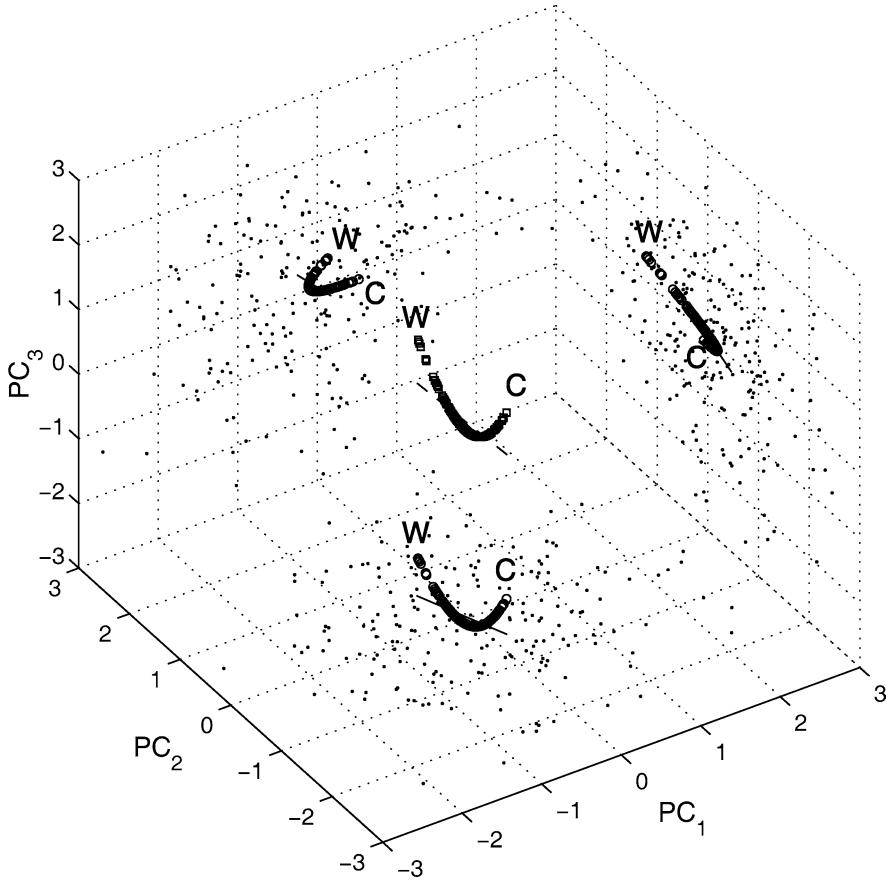

Fig. 3 The SLP response to the ENSO SST index extracted by the NN projection shown as a *thick curve* of overlapping squares in the PC_1–PC_2–PC_3 3-D space (the PCs have been standardized). The linear response is shown as a *dashed straight line*. The SLP signal is also projected onto the PC_1–PC_2, PC_2–PC_3 and PC_1–PC_3 planes, where the nonlinear projection is presented by the curves of *overlapping circles*, the linear projection by *thin solid lines*, and the projected data points by the scattered dots. The labels "*C*" and "*W*" denote the extreme cold and warm states respectively

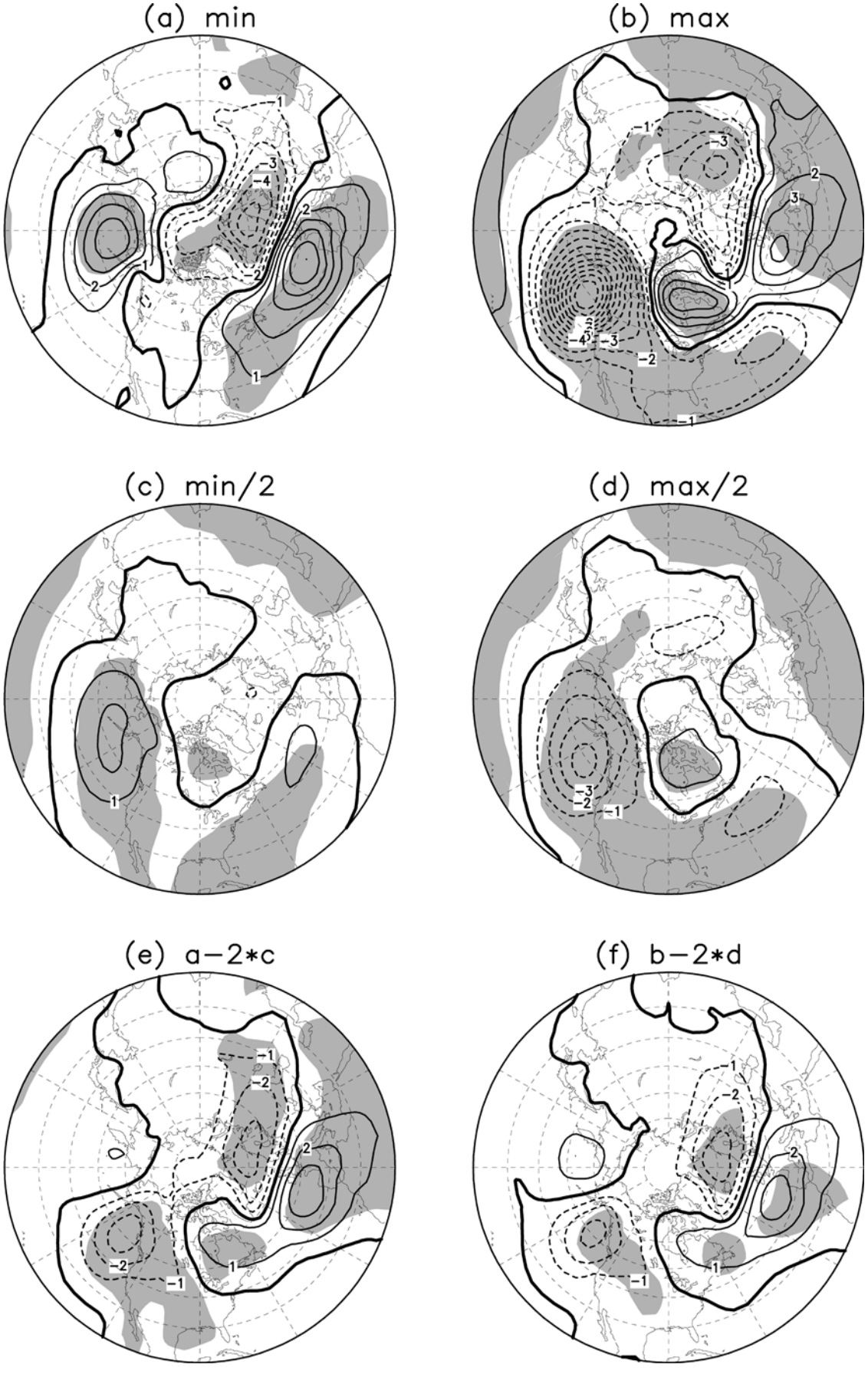
(a) min
(b) max
(c) min/2
(d) max/2
(e) a−2*c
(f) b−2*d

America to western Europe, and significant negative SLP anomalies over Scandinavia and Iceland, extending to eastern Europe, resembling the positive phase of the NAO pattern, consistent with the composite SLP anomaly pattern by Pozo-Vázquez et al. (2001). When the SST index takes on its maximum value (i.e. strong El Niño), the positive SLP anomalies over North Pacific in Fig. 4a have turned into negative anomalies (Fig. 4b), with the anomaly center shifted eastward by 35° and with magnitude increased, confirming the nonlinear impact of ENSO on the North Pacific and North America winter climate as documented by previous studies (e.g. Hoerling et al. 1997). Meanwhile, the positive SLP anomalies over North Atlantic are maintained and separated into two centers—one over eastern Canada, and the other one over western Europe (Fig. 4b). Relative to the SLP pattern shown in Fig. 4a, Fig. 4b still displays a positive NAO-like pattern over the Euro-Atlantic sector, but with the positive and negative anomaly centers shifted eastward by about 15° and 30° respectively. Despite relatively weaker magnitude and meridional gradient over North Atlantic and Europe in Fig. 4b compared to Fig. 4a, the NN projection reveals significant SLP anomalies over the Euro-Atlantic region during strong warm ENSO episodes, different from the composite analysis by Pozo-Vázquez et al. (2001), where no significant SLP anomalies were found over North Atlantic during warm episodes. The similarity (or poor anti-symmetry) in the SLP anomaly pattern over the Euro-Atlantic region between Figs. 4a and b suggests a strong nonlinear relation between ENSO and the Euro-Atlantic winter climate.

Table 1 shows the PC values derived from the NN projection when the SST index takes on its minimum and maximum values, where we see that large negative SST index values concur with large positive PC_1, small positive PC_2, small negative PC_3 and large positive PC_4; while large positive SST index values concur with small positive PC_1, large positive PC_2, intermediate positive PC_3 and small negative PC_4. When the SST index varies from its minimum value to its maximum value, the SLP response moves smoothly along the 3-D curve in Fig. 3 from the end labelled "C" to the other end "W" (corresponding to the extreme cold and warm states respectively). From the corresponding EOFs (Fig. 1), one can easily understand how the asymmetric SLP anomaly patterns arose during the extreme cold and warm states as shown in Figs. 4a, b. Figure 4a roughly resembles the positive EOF1, while Fig. 4b is basically a combination of positive EOF2 and positive EOF3. The asymmetric response between extreme cold and warm episodes is also contributed by higher modes although their amplitudes are relatively small.

The SLP anomalies associated with the half minimum and half maximum SST index are shown in Figs. 4c and d, respectively. The SLP anomalies decrease in magnitude, especially over the Euro-Atlantic region. The anti-symmetry between Figs. 4c and d is much more conspicuous than that between Figs. 4a and b, suggesting that appreciable SSTA are required for initiating the nonlinear atmospheric response.

To estimate the nonlinear response in the SLP anomalies to the tropical SSTA, we plotted in Fig. 4e the difference between the SLP anomalies in Fig. 4a and twice the anomalies in Fig. 4c; and similarly in Fig. 4f, the difference between the anomalies in Fig. 4b and twice the anomalies in Fig. 4d. Interestingly, despite the large difference between Figs. 4a and b, and the smaller difference between Figs. 4c and d, the SLP anomalies in Figs. 4e and f agree well with each other, indicating that regardless of the sign of the SST index, the nonlinear response has positive SLP anomalies appearing over North Atlantic and western Europe, and negative SLP anomalies over Scandinavia and Iceland, resembling a positive NAO pattern. In addition, we see negative SLP anomalies over the west coast of North America and weak positive anomalies over eastern Canada, which contributes to the nonlinear response of North America climate to ENSO.

To test the robustness of these results, we repeated our bootstrap calculations by deleting the two winters with the strongest ENSO warm episodes (1982–1983, 1997–1998), and the two winters with the strongest cold episodes (1973–1974, 1975–1976) from the data record. Even without the extreme ENSO episodes, the resulting NN projection yielded basically the same patterns as in Fig. 4. Another test involved removing the two winters with the strongest positive NAO episodes (1958–1959, 1988–1989; selection is based on the NAO index, i.e. the first PC of the SLP anomalies over Northern Hemisphere (Hurrell et al. 2003)), and the two winters with the strongest negative NAO episodes (1968–1969, 1976–1977), which also gave similar NN projection results, thereby confirming that the nonlinear response found by our NN projection was not the result of fitting to one or two extreme cases.

3.2 The linear and nonlinear component of the SLP response

The SLP response to the ENSO SSTA as extracted by the NN projection can be separated into a linear component, i.e. the linear projection (the straight line in Fig. 3), and a nonlinear component—the residual after the linear projection subtracted from the NN projection, i.e. the 11 PCs from the NN projection minus the 11 PCs from the linear projection. The resulting 11 PCs for the linear and nonlinear components can then be combined with the corresponding EOFs to yield the linear and nonlinear responses of SLP to ENSO. The linear and nonlinear components account for 65 and 35% of the variance in the NN projected SLP anomaly data respectively.

Principal component analysis is used to separately analyze the linear and nonlinear response field of SLP anomalies during January 1950 – March 2003, where over 99% of the variance for either data field can be

Table 1 The standardized PC values derived from the NN projection when the ENSO SST index takes on its minimum and maximum values

SLP PC	STD	NN(min)	NN(max)
1	49.69	0.520	0.130
2	36.18	0.081	1.217
3	34.71	−0.117	0.382
4	31.28	0.656	-0.144
5	28.47	0.238	0.330
6	27.68	−0.379	0.419
7	23.41	−0.582	0.244
8	21.11	0.483	1.019
9	19.62	0.040	1.295
10	16.56	−0.045	−0.794
11	15.07	0.344	−0.158

The standard deviation (STD) of the PCs is also given

explained by its first PCA mode. For the linear response field, the high percentage variance explained by the first PCA mode is not surprising since the SLP anomalies field was generated originally by linearly projecting from a single SST index time series. For the nonlinear response field, the high percentage variance explained by a single PCA mode is due to the fact that the nonlinear response is very simple, consisting of mainly a quadratic response, as will be shown later. When the PC1 of the linear response (the solid line in Fig. 5a) takes on a positive value, the EOF1 of the linear response (Fig. 5b) shows negative SLP anomalies appearing over North Pacific and the west coast of North America continent, and weak positive SLP anomalies over eastern Canada, with much weaker anomalies over the Euro-Atlantic area, indicating the linear impact of ENSO on the SLP over the Euro-Atlantic sector is not important. However, the EOF1 of the nonlinear response (Fig. 5c) shows notable SLP anomalies over the Euro-Atlantic region, which resemble a positive NAO pattern, and are similar to the SLP anomaly patterns shown in Figs. 4e, f, suggesting the Euro-Atlantic winter climate mainly responds to ENSO nonlinearly. The PC1 of the linear

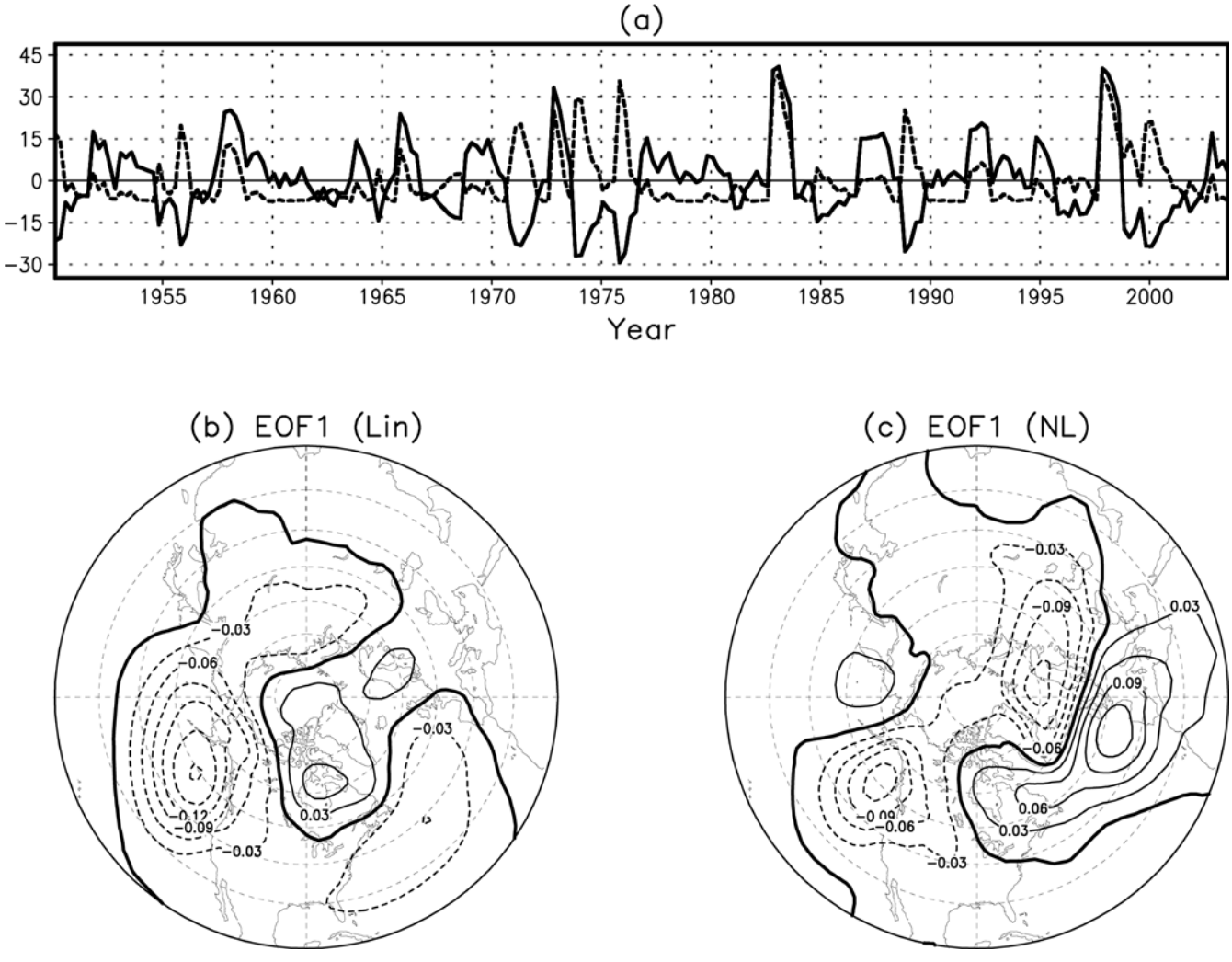

Fig. 5 **a** The leading PC of the SLP anomalies from the linear and nonlinear response to the ENSO SST index as extracted by the NN projection, shown by the *solid line* and *dashed line*, respectively. The corresponding PCA spatial patterns for linear and nonlinear components are shown in panels **b** and **c**, respectively. The contour interval is 0.03, and the spatial modes have been normalized to unit norm

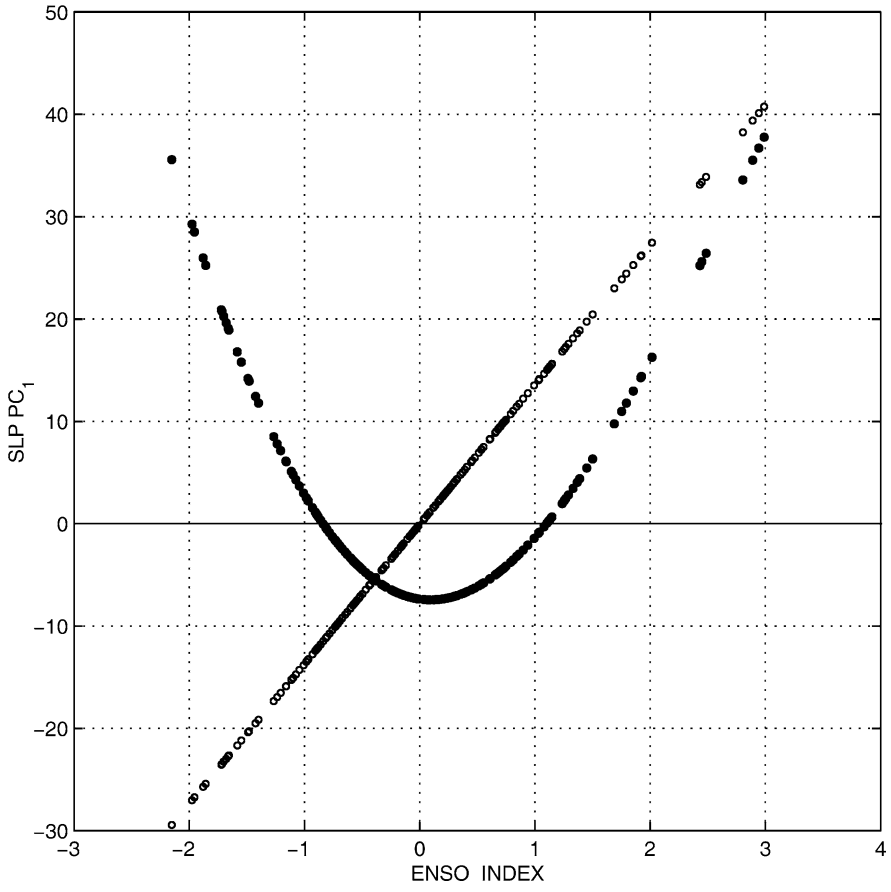

Fig. 6 The scatter plots between the ENSO SST index and the EOF PC1 of the nonlinear response shown by the curve of small *solid circles*. The linear response is shown by the straight line of *open circles*

response is synchronous with the ENSO SST index, while the PC1 of the nonlinear response (the dashed line in Fig. 5a) has positive values not only during the El Niño winters (1958, 1966, 1973, 1983, 1992 and 1998), but also during La Niña winters (1950, 1956, 1971, 1974, 1976, 1989, 1999 and 2000). Hence, regardless of warm or cold episodes, the SLP has the same response pattern as depicted by Fig. 5c. This leads to a positive NAO-like SLP pattern for both extreme cold and warm episodes (Figs. 4a, b), showing the linear response (Fig. 5b) is weak over the Euro-Atlantic region.

The scatter plots between the PC1 of the nonlinear response and the SST index are shown in Fig. 6 by the parabola-like curve of small solid circles, which can be fitted well by the polynomial function $\mathrm{PC}_1^{\mathrm{NL}} = -7.37 - 1.55x + 8.28x^2 - 0.54x^3 - 0.19x^4 + 0.01x^5$, where x is the ENSO SST index, suggesting that the nonlinear response of SLP to ENSO is mainly a quadratic response. For comparison, the scatter plot of the linear response is fitted well by the straight line $\mathrm{PC}_1^{\mathrm{Lin}} = 13.65x$.

3.3 A polynomial study

To further illuminate the nonlinear response of the SLP anomalies, we consider a polynomial fit of the SST index to the SLP anomaly at each grid point. Let T be the SST index, and $x_n = T^n$, then p, the original SLP anomaly at a grid point with linear trend removed, was fitted by $p = a_0 + a_1\hat{x}_1 + a_2\hat{x}_2 + \cdots + a_N\hat{x}_N$, where $\hat{x}_n$ is x_n normalized. For 400 bootstrap samples and for each spatial point of the SLP anomaly field, regression coefficients $a_0,\ldots,a_N$ were computed. After ensemble-averaging over all bootstrap samples, a_n provided the spatial pattern associated with the nth order response to the SST index. When tested over independent data (i.e. data not selected in a bootstrap sample), the smallest MSE (averaged over all bootstrap samples) was found when $N = 2$, indicating overfitted results when $N > 2$. Hence, there is no evidence for cubic or higher order nonlinear response to ENSO. With $N = 2$, the ensemble-averaged values of a_1 and a_2 are plotted in Fig. 7.

Again the linear term has major SLP anomalies over North Pacific, and rather weak SLP anomalies over the Euro-Atlantic region (Fig. 7a). In contrast, the quadratic term (Fig. 7b) shows major SLP anomalies over Euro-Atlantic, resembling a positive NAO pattern, basically consistent with Fig. 5c, as well as Figs. 4e, f, confirming that nonlinear response of SLP to ENSO is mainly a quadratic response.

4 Summary and discussion

A fully nonlinear projection of the ENSO SST index to the Northern Hemisphere winter (December to March) SLP monthly anomalies has been achieved using NNs. Statistically significant SLP anomalies resembling a po-

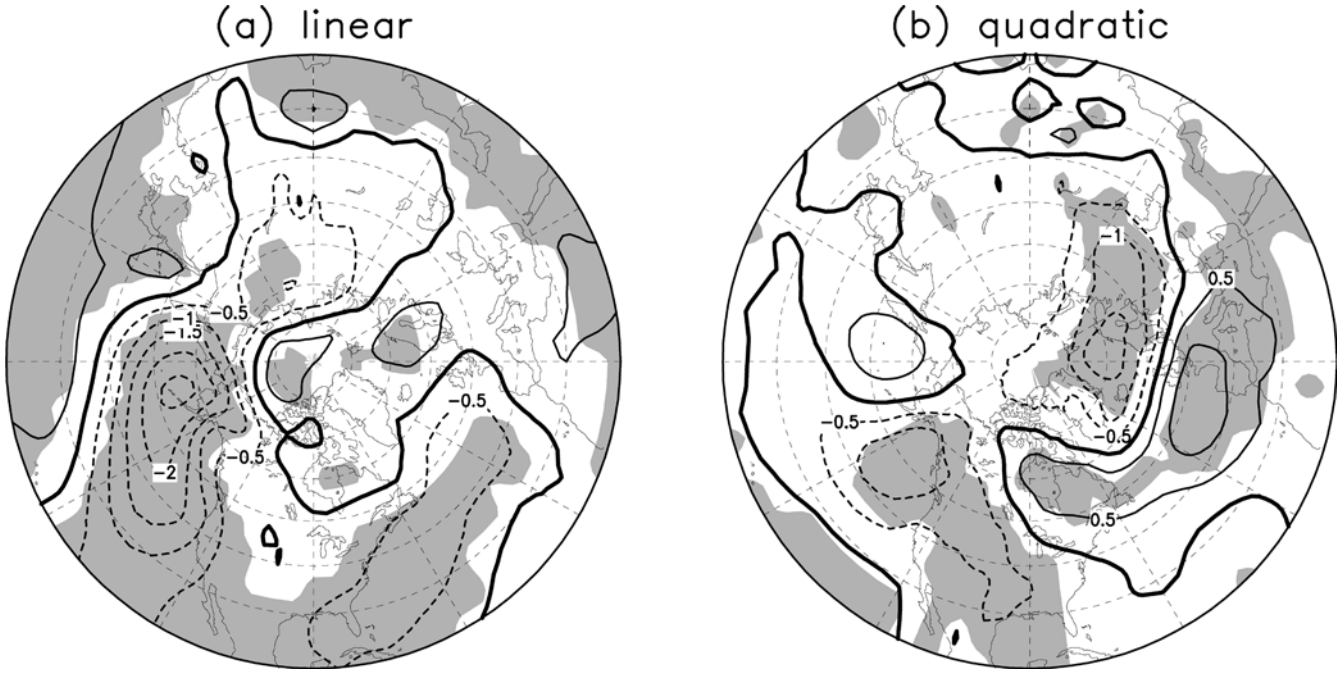

Fig. 7 The SLP anomaly patterns associated with the **a** linear and **b** quadratic terms of the tropical Pacific SST index. The contour interval is 0.5 hPa and the *shaded areas* indicate statistical significance at the 5% level from bootstrapping

sitive NAO pattern are found over the Euro-Atlantic sector during both extreme warm and cold episodes, except that the positive SLP anomaly center over the North Atlantic is shifted eastward by approximately 15° during warm episode relative to that during cold episode. The SLP anomalies from the NN projection consist of a linear part, which has anomalies largely confined over North Pacific and the west coast of North America, and a nonlinear part, which has major positive SLP anomalies over North Atlantic and western Europe, and negative SLP anomalies over Scandinavia and Iceland, resembling the positive phase of the NAO pattern. A polynomial study further indicates this nonlinear component to be a quadratic response to the SSTA. This manifestation of the positive phase of the NAO during extreme warm and cold ENSO episodes was also found in the winter 500 mb geopotential height anomalies (Wu and Hsieh 2004).

What needs to be emphasized is that, unlike the response of the North American climate to ENSO, where the linear component is important, the response of the Euro-Atlantic climate to ENSO is mainly nonlinear. This is probably why previous studies using linear analysis failed to obtain a robust relationship between ENSO and NAO.

How the Euro-Atlantic climate anomalies are physically linked to the tropical Pacific ENSO SSTA is still an open question. Just as its name implies, the Pacific–North America (PNA) teleconnection (Wallace and Gutzler 1981), which is based on linear large-scale wave theory (Hoskins and Karoly 1981), cannot cover the Euro-Atlantic region (Figs. 5b and 7a). A possible mechanism is the wave–wave interaction in the midlatitudes, e.g. the synoptic eddies and stationary waves. Merkel and Latif (2002) showed that a high resolution AGCM, which can represent more realistically the transient eddy activity, is necessary to simulate the cyclone variability related to ENSO over the North Atlantic/European region. Although the physical process was not given in detail, their results agree with the our finding here that the Euro-Atlantic climate is nonlinearly connected to ENSO. Thus, the SST changes in the tropical Pacific Ocean is still an important source for the predictability of the Atlantic and European climate. The relative importance of the impact of ENSO SST and the Atlantic SST anomalies on the Euro-Atlantic climate will be discussed in future work.

Acknowledgements The authors acknowledge the support from the Natural Sciences and Engineering Research Council of Canada via research and strategic grants.

References

Bishop CM (1995) Neural networks for pattern recognition. Clarendon, Oxford

Cassou C, Terray L (2001) Oceanic forcing of the wintertime low-frequency atmospheric variability in the North Atlantic European sector: a study with the ARPEGE model. J Clim 14:4266–4291

Deser C, Blackmon ML (1995) On the relationship between tropical and North Pacific sea surface temperature variations. J Clim 8:1677–1680

Dong B-W, Sutton RT, Jewson SP, O'Neill A, Slingo JM (2000) Predictable climate in the North Atlantic sector during the 1997–1999 ENSO cycle. Geophys Res Lett 27:985–988

Efron B, Tibshirani RJ (1993) An introduction to the bootstrap. CRC, Boca Raton

Fraedrich K (1994) An ENSO impact on Europe? Tellus 46A:541–552

Fraedrich K, Müller K (1992) Climate anomalies associated with ENSO extremes. Int J Climatol 12:25–31

Halpert MS, Ropelewski CF (1992) Surface temperature patterns associated with the Southern Oscillation. J Clim 5:577–593

Hoerling MP, Kumar A, Zhong M (1997) El Niño, La Niña and the nonlinearity of their teleconnections. J Clim 10:1769–1786

Hoerling MP, Kumar A, Xu T (2001a) Robustness of the nonlinear climate response to ENSO's extreme phases. J Clim 14:1277–1293

Hoerling MP, Hurrell J, Xu T (2001b) Tropical origins for recent North Atlantic climate change. Science 292:90–92

Hoskins B, Karoly D (1981) The steady linear response of a spherical atmosphere to thermal and orographic forcing. J Atmos Sci 38:1179–1196

Hsieh WW (2001) Nonlinear canonical correlation analysis of the tropical Pacific climate variability using a neural network approach. J Clim 14:2528–2539

Hsieh WW (2004) Nonlinear multivariate and time series analysis by neural network methods. Rev Geophys 42:RG1003. DOI 10.1029/2002RG000112

Hsieh WW, Tang B (1998) Applying neural network models to prediction and data analysis in meteorology and oceanography. Bull Am Meteorol Soc 79:1855–1870

Huang J-P, Higuchi K, Shabbar A (1998) The relation between the North Atlantic Oscillation and El Niño-Southern Oscillation. Geophys Res Lett 25:2707–2710

Hurrell JW, Kushnir Y, Ottersen G, Visbeck M (2003) An Overview of the North Atlantic Oscillation. In: Hurrell JW, Kushnir Y, Ottersen G, Visbeck M (eds) The North Atlantic Oscillation: climate significance and environmental impact. Geophys Monogr Ser 134:1–35

Merkel U, Latif M (2002) A high resolution AGCM study of the El Niño impact on the North Atlantic/European sector. Geophys Res Lett 29:1291–1294. DOI 10.1029/2001GL013726

Montroy DL, Richman MB, Lamb PJ (1998) Observed nonlinearities of monthly teleconnections between tropical Pacific sea surface temperature anomalies and central and eastern North American precipitation. J Clim 11:1812–1835

Pozo-Vázquez D, Esteban-Parra MJ, Rodrigo FS, Castro-Dáez Y (2001) The association between ENSO and winter atmospheric circulation and temperature in the North Atlantic region. J Clim 14:3408-3420

Raible CC, Blender R (2004) Northern hemisphere midlatitude cyclone variability in GCM simulations with different ocean representations. Clim Dyn 22:239–248. DOI 10.1007/s00382-003-0380-y

Rogers JC (1984) The association between the North Atlantic Oscillation and the Southern Oscillation in the Northern Hemisphere. Mon Wea Rev 112:1999–2015

Shabbar A, Bonsal B, Khandekar M (1997) Canadian precipitation patterns associated with Southern Oscillation. J Clim 10:3016–3027

Smith TM, Reynolds RW (2003) Extended reconstruction of global sea surface temperatures based on COADS data (1854–1997). J Clim 16:1495–1510

Sutton RT, Hodson DLR (2003) Influence of the Ocean on North Atlantic climate variability 1981–1999. J Clim 16:3296–3313

Thompson DWJ, Wallace JM (1998) The Arctic Oscillation signature in the wintertime geopotential height and temperature fields. Geophys Res Lett 25:1297–1300

Thompson DWJ, Wallace JM (2000) Annular modes in the extratropical circulation. Part I: month-to-month variability. J Clim 13:1000–1016

Trenberth KE, Paolino DA (1980) The Northern Hemisphere sea level pressure data set: trends, errors and discontinuities. Mon Wea Rev 108:855–872

Trenberth KE, Branstator GW, Karoly D, Kumar A, Lau N-C, Ropelewski C (1998) Progress during TOGA in understanding and modelling global teleconnections associated with tropical sea surface temperatures. J Geophys Res 103:14291–14324

Wallace JM, Gutzler D (1981) Teleconnection in the geopotential height filed during the Northern Hemisphere winter. Mon Wea Rev 109:784–812

Wu A, Hsieh WW (2004) The nonlinear Northern Hemisphere winter atmospheric response to ENSO. Geophys Res Lett 31:L02203. DOI 10.1029/2003GL018885

Wu A, Hsieh WW, Zwiers FW (2003) Nonlinear modes of North American winter climate variability derived from a general circulation model simulation. J Clim 16:2325–2339